

## Supporting Information

### **Freestanding interlayers for Li-S batteries: Design and synthesis of hierarchically porous N-doped C nanofibers comprising vanadium nitride quantum dots and MOF-derived hollow N-doped C nanocages**

*Rakesh Saroha,<sup>a</sup>, Jang Hyeok Oh,<sup>a</sup> Young Hoe Seon,<sup>a</sup> Yun Chan Kang,<sup>b</sup> Jae Seob Lee,<sup>a</sup> Do Won Jeong,<sup>a</sup> and Jung Sang Cho<sup>\*a</sup>*

<sup>a</sup> Department of Engineering Chemistry, Chungbuk National University, Chungbuk 361-763, Republic of Korea

<sup>b</sup> Department of Materials Science and Engineering, Korea University, 145, Anam-Ro, Seongbuk-Gu, Seoul 02841, Republic of Korea

\* Corresponding author.

E-mail: jscho@cbnu.ac.kr Tel.: +82-43-261-2489. Fax: +82-43-262-2380. (Jung Sang Cho)

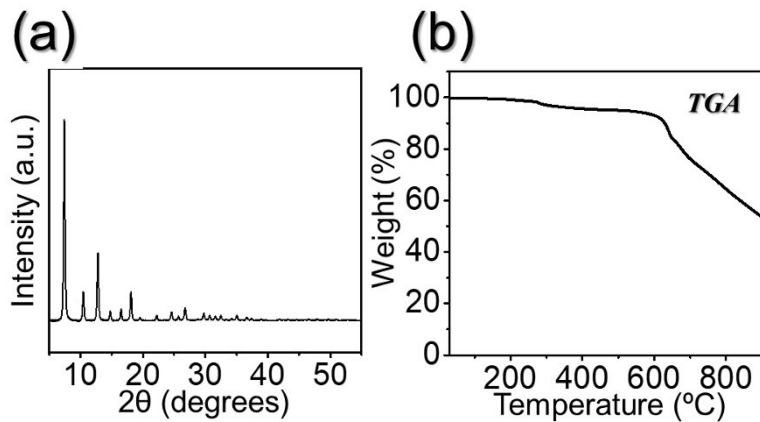


**Fig. S1.** (a) XRD pattern and (b) TG curve under N<sub>2</sub> atmosphere of the as-prepared ZIF-8 polyhedra.

#### ZIF- 8 decomposition reaction:

The possible reaction involved for the disintegration of ZIF-8 at high temperature of 800 °C can be as:

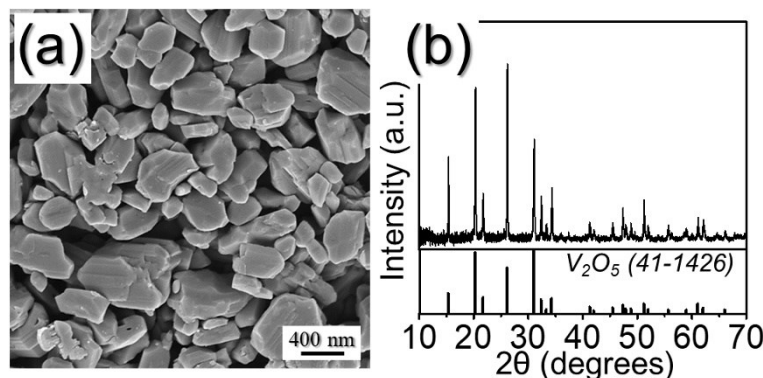
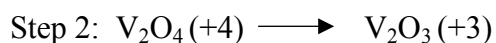
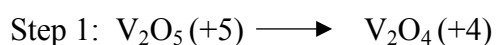


**Fig. S2.** (a) FE-SEM image and (b) XRD pattern of the commercial V<sub>2</sub>O<sub>5</sub> powders as a vanadium nitride precursor.

#### Reaction mechanism:

Intermediate by-products involved during the carbonitrothermic reduction conversion reaction of V<sub>2</sub>O<sub>5</sub> to VN:



The number within the parenthesis represents the oxidation state of vanadium.

The overall reaction involved during the carbonitrothermic reduction conversion can be written as:



Besides, the decomposition of the urea and subsequent conversion to nitrogen can be represented in the reactions below:

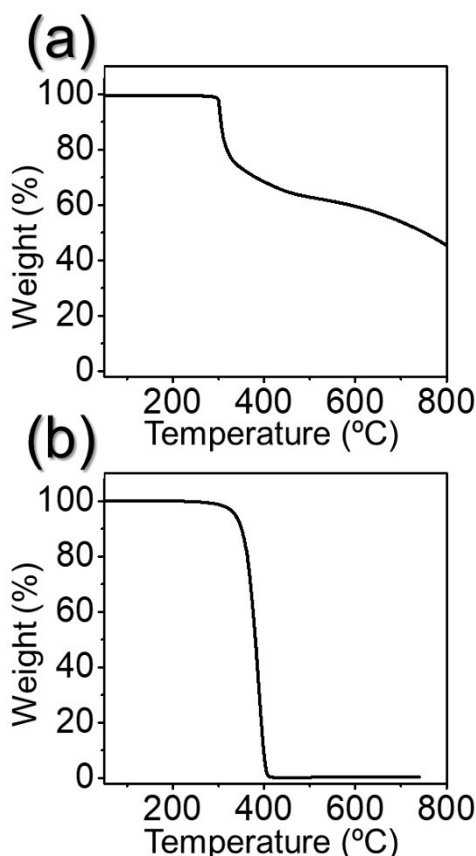
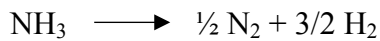
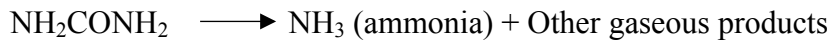


**Fig. S3.** TG curves of (a) PAN and (b) PS granules performed under N<sub>2</sub> atmosphere.

TG curve of PAN (Fig. S3a) clearly indicates a steep weight loss around 300 °C suggesting conversion of PAN into C. However, as temperature increases, the weight loss gets slower and at 800 °C, the whole polymer seems to convert into C with a total weight left around 50 wt.%. Likewise, the TG curve of PS indicates single step weight loss which starts around 320 °C and finishes at 410 °C, suggesting complete removal of PS with no residue left over.

**Table S1.** Quantitative analysis of N-CNF@VN/HNC, N-CNF@HNC, and N-CNF interlayers for Li-S batteries using TGA and elemental analysis (EA).

Sample	Vanadium Nitride wt. (%)	Carbon wt. (%)	Nitrogen wt. (%)
<b>N-CNF@VN/HNC</b>	8.5	81.3	10.2
<b>N-CNF@HNC</b>	-	86.9	13.1
<b>N-CNF</b>	-	88.7	11.3

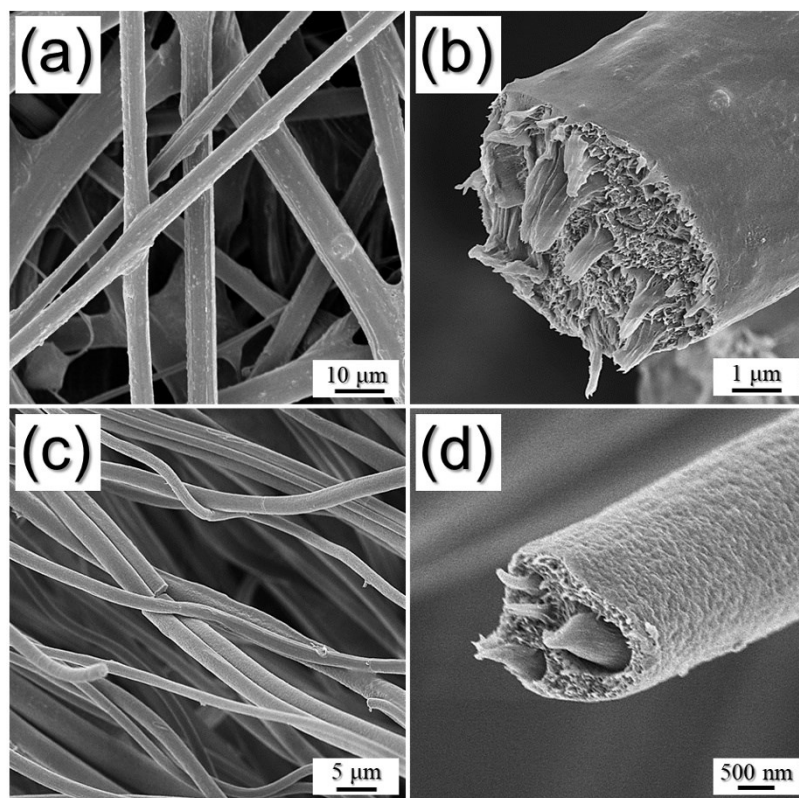


**Fig. S4.** FE-SEM images of (a,b) as-spun ZIF-8/PAN/PS composite fibers and (c,d) as-spun PAN/PS composite fibers before heat-treatment.

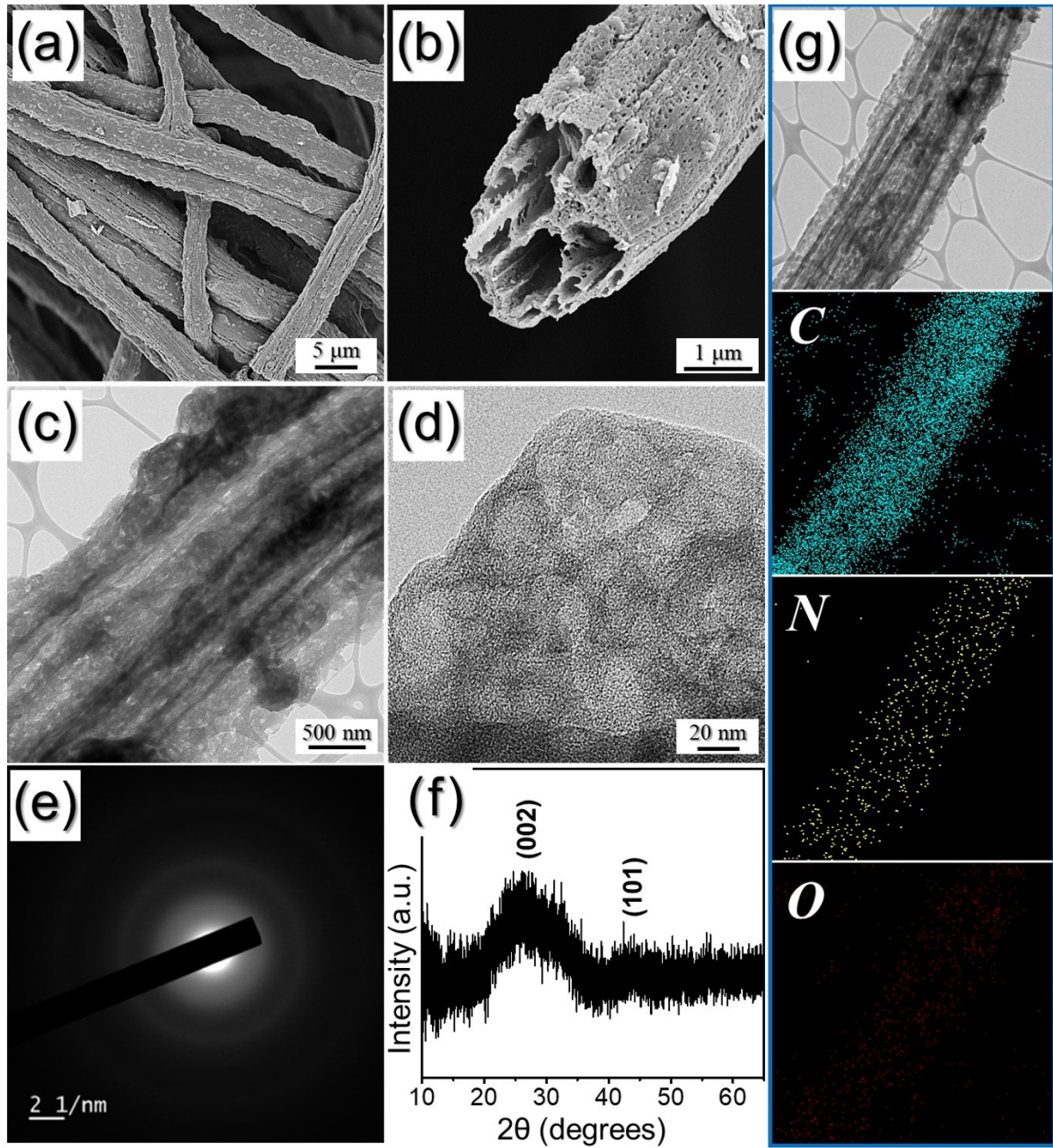


**Fig. S5.** Morphologies, SAED, and XRD pattern, and elemental mapping images of N-CNF@HNC nanofibers obtained after heat-treatment of as-spun ZIF-8/PAN/PS composite fibers at 800 °C: (a,b) FE-SEM image, (c,d) HR-TEM images, (e) SAED pattern, (f) XRD pattern, and (g) elemental mapping images.

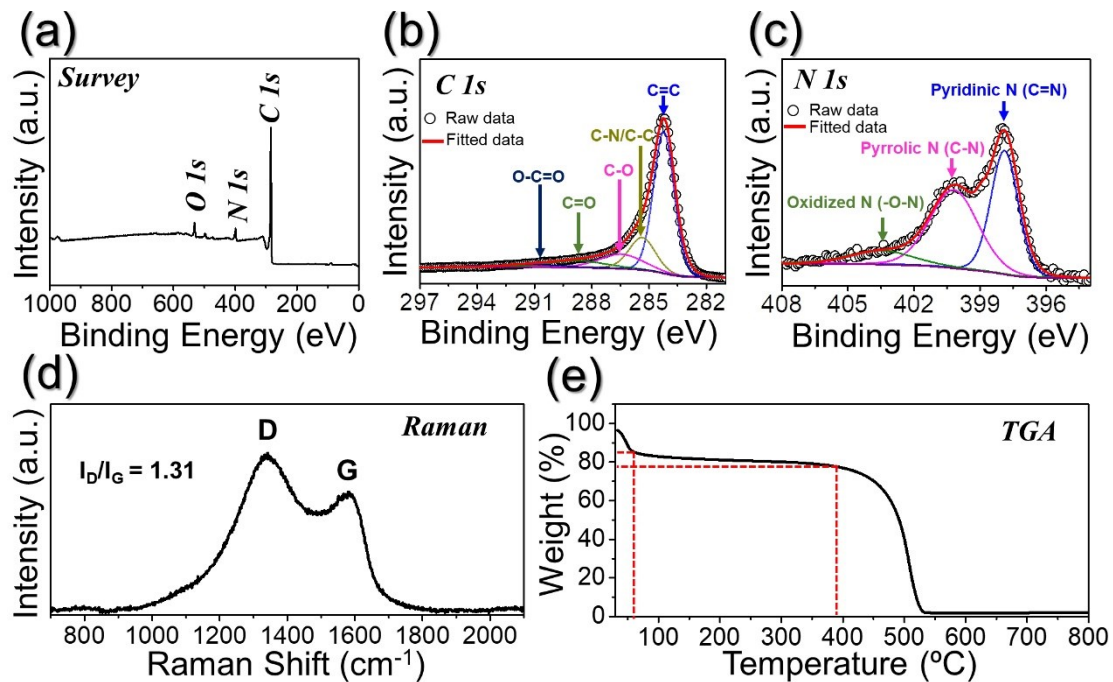


**Fig. S6.** (a) XPS survey spectrum, (b) C 1s XPS spectrum, (c) N 1s XPS spectrum, (d) Raman spectrum, and (e) TG curve of N-CNF@HNC nanofibers.

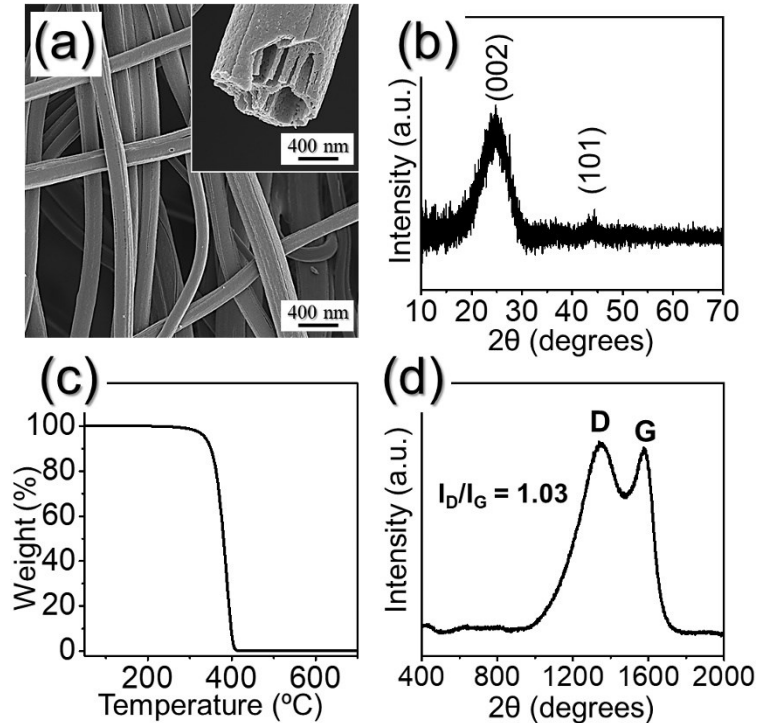


**Fig. S7.** Characteristics of N-CNF nanofibers obtained after heat-treatment of as-spun PAN/PS composite fibers at 800 °C: (a) FE-SEM images, (b) XRD pattern, (c) TG curve, and (d) Raman spectrum.

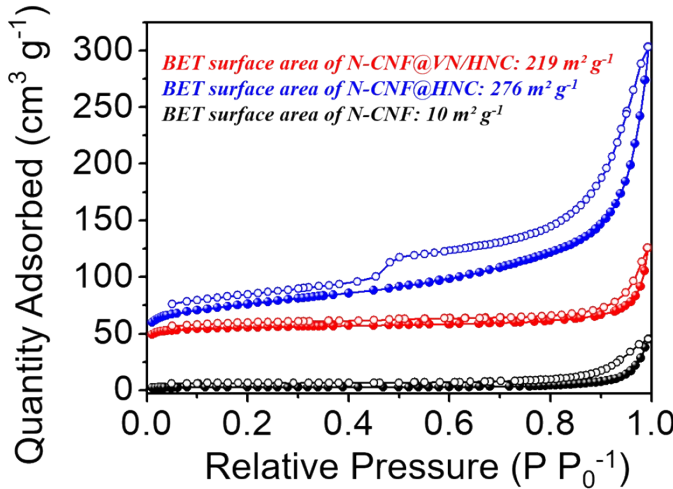


**Fig. S8.**  $\text{N}_2$  adsorption-desorption isotherms of N-CNF@VN/HNC, N-CNF@HNC, and N-CNF nanofibers.

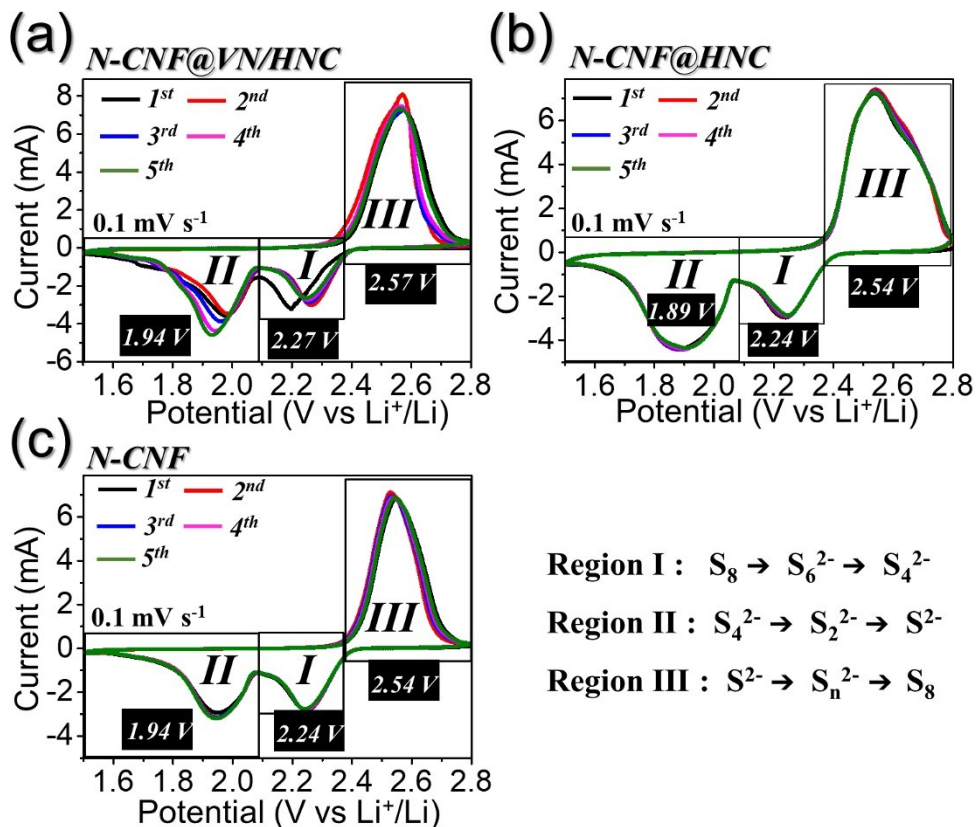


**Fig. S9.** CV curves of Li-S cells with different interlayers arrangement for initial five cycles at a scan rate of  $0.1 \text{ mV s}^{-1}$ : (a) N-CNF@VN/HNC, (b) N-CNF@HNC, and (c) N-CNF nanofibers.

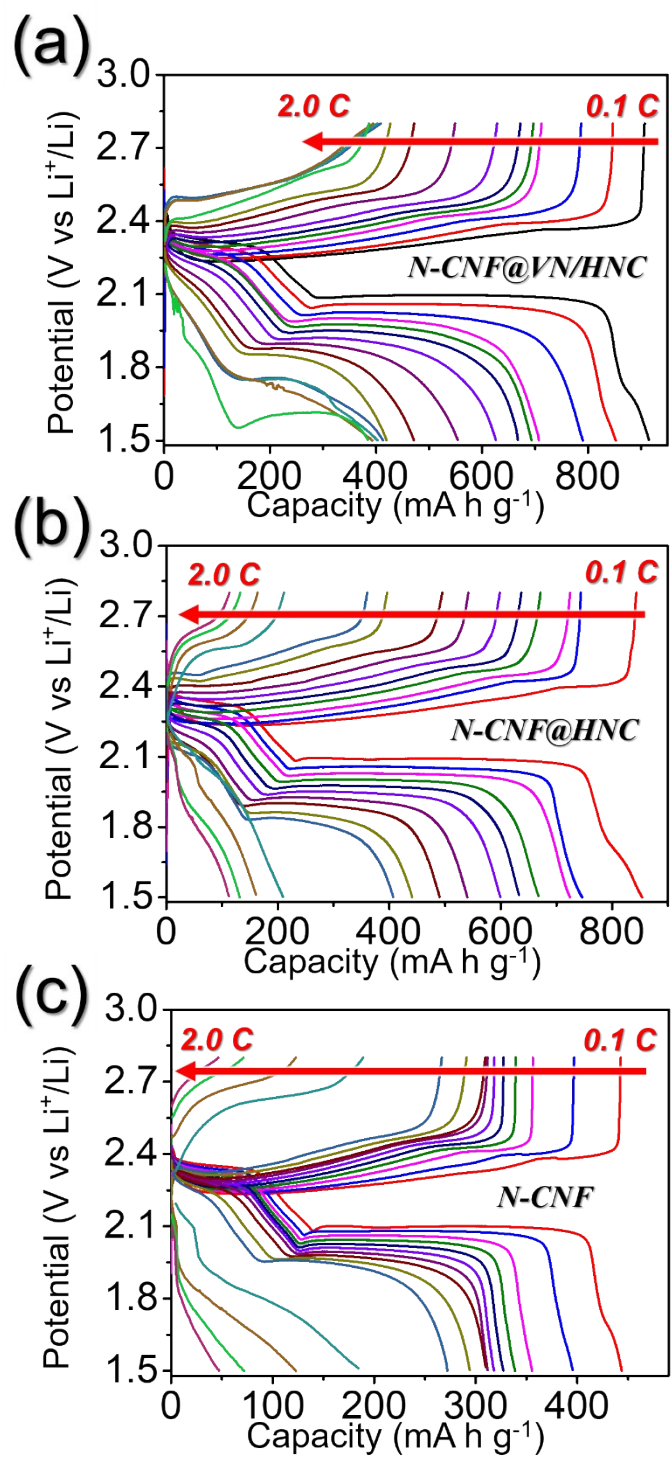


**Fig. S10.** Respective charge-discharge profiles of Li-S cells with different interlayer arrangements at various C-rates: (a) N-CNF@VN/HNC, (b) N-CNF@HNC, and (c) N-CNF nanofibers.

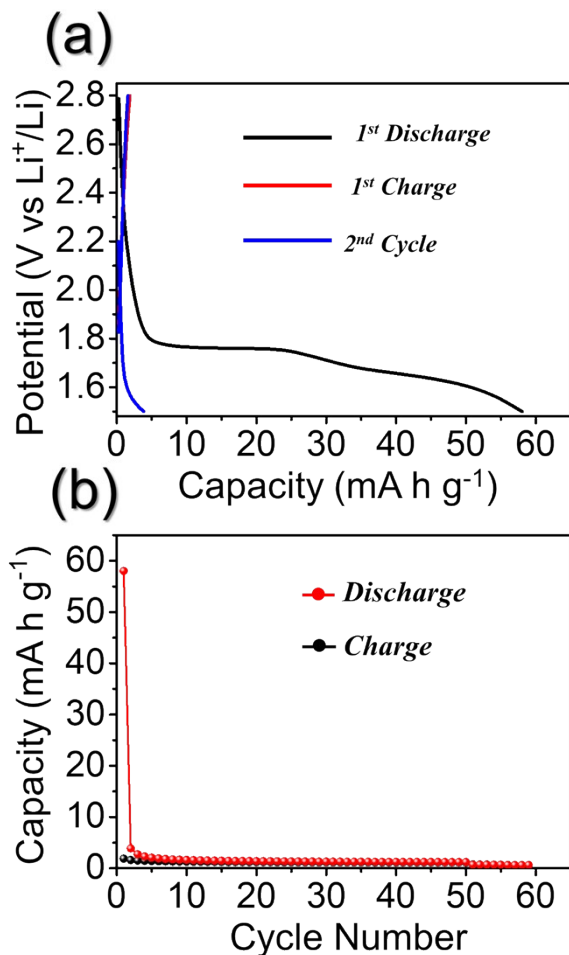


**Fig. S11.** Capacity contribution of N-CNF@VN/HNC electrode only vs.  $\text{Li}^+/\text{Li}$  at a current density of  $100 \text{ mA g}^{-1}$ .

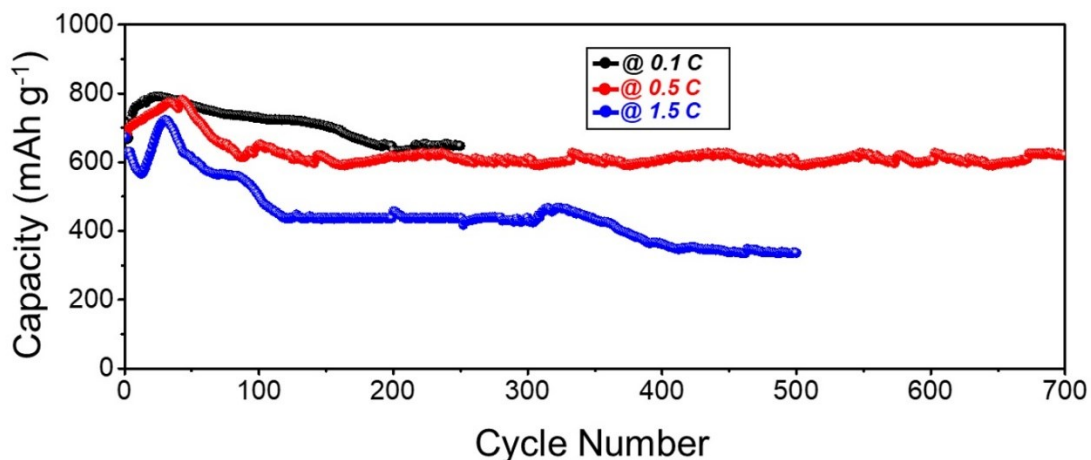


**Fig. S12.** Extended cycling performance of the Li-S cells featuring N-CNF@VN/HNC interlayer at 0.1, 0.5, and 1.5 C-rate.

**Table S2.** Comparison table of the electrochemical performances obtained in the present work with the previously reported results.

Cathode	interlayer	Interlayer loading (mg cm <sup>-2</sup> )	Sulfur content in electrode/loading (wt.-%/ mg cm <sup>-2</sup> )	Initial C <sub>discharge</sub> /Rate [mAh g <sup>-1</sup> /C]	Final Discharge Capacity/Rate /Cycle No. [mAh g <sup>-1</sup> /C/-]	Ref
Sulfur	N-CNF@VN/HN C	2.6	52.6/4.0*	1103/0.05	646/0.1/200	This Work
			63.7/ 8.2*	833/0.05	610/0.5/500	
			67.1/11.0*	776/0.05	374/1.0/500	
Sulfur/CNT composite	Porous VN coated separator	1.52	63/1.4-1.6	1050/0.5 960/1.0	539/0.05/100 456/0.05/100	[1]
BNT-S	Fe <sub>3</sub> C/BNT	-	68/1.8-2.0	1235/0.1	550/0.5/500	[2]
Sulfur	SnO <sub>2</sub> NWs@CP	1.0	70/2.2	900/0.2	886/0.2/100	[3]
Sulfur	Fe <sub>3</sub> C-CNF	0.7-1.0	70/2.0	1087/0.2	941/0.2/100 804/1.0/250	[4]
S/C	FS-SiO <sub>2</sub> /C-CNF	4-5***	56/1.0	1298/0.1	900/50/0.1	[5]
Sulfur	1T-MoS <sub>2</sub> /CNF	-	60/1.0	880/0.1	718/100/0.1	[6]
Sulfur	Pyrolyzed pencil coated interlayer	0.16	70/-	862/1000**	725/350/1000*	[7]
Sulfur	Free-standing carbon nanofibers	0.38	75/1.8	1120/0.1	850/100/0.1	[8]
Sulfur	Phosphorous doped carbonized cotton cloth	3.16	60/1.0	1407/0.2	648/800/1.0	[9]
Sulfur	VN-Nanowires	-	80/1.9	1192/0.5	878/300/0.5	[10]
S/CB	WO <sub>3</sub> @NS-CNFs	1.0	54.4/1.5	1444/0.2	870/200/0.5	[11]
S/RGO	ZnO/CNT/RGO	0.85	-/1.7	1061/0.2	768/150/0.2	[12]
Sulfur	N, S-doped hierarchical biomass porous carbons	-	80/1.8	1549/0.1	609/300/0.5	[13]
Sulfur	G/MoO <sub>3</sub> -Mo	2.04	70/1.54	1288/0.2	1063/100/0.2	[14]
Sulfur	MoS <sub>2</sub> /graphene	0.5	60/0.8-1.2	1642/200**	720/100/200*	[15]
Sulfur	N,S-codoped graphene	1.6-2.0	60/2.0	-	724/110/3.0	[16]
Sulfur	Activated carbon	1.0	70/2.5	1200/0.1	897/100/0.1	[17]

nanofiber						
S/C composite	C@Ti <sub>4</sub> O <sub>7</sub> CNFs	1.0	63/1.5	1000/1.0	721/200/1.0	[18]
S/CNTs	Tin-modified carbon-skeleton	0.42	70/1.3-1.5	1021/1.0	654/400/1.0	[19]
CMK-3/S	ZIF/CNFs	0.3	60/2.3	1406/0.5	553/300/0.5	[20]
S/C	N-C-Co	0.3	60/1.5	1216/1.0	660/250/1.0	[21]
Sulfur	3D CCF	-	70/2.0	1347/0.1	1077/100/0.1	[22]
S/C	PC-Fe <sub>3</sub> O <sub>4</sub> @rGO-graphite	-	52.5/1-1.2	1242/0.5	495/1000/0.5	[23]
3DNPC/VN-S	-		-/0.75	1156/0.2	734/1.0/300	[24]
S/MVN@C NWs	-		57.2/2.8	1300/0.2	636//1.0/200	[25]
Al-S-VGCF	-		-/2.03 -/5.40	1100/50** 980/50**	616/100/100* 650/100/100*	[26]
VN@C/S	-		57.2/1.2-1.5 57.2/4.2	1350/0.1 1200/0.2	789/0.5/100 592/1.0/300 890/0.2/100	[27]
Co-VN@C/S	-		-/1.3-1.5	1379/0.1	715/0.5/200 600/1.0/300	[28]

‘\*’ The sulfur content in the present work is the effective sulfur wt.% including the interlayer mass, which was calculated using the following relation:

$$\text{Sulfur mass in the electrode}$$

$$\text{Effective sulfur wt.\%} = \frac{\text{Electrode mass without aluminum foil} + \text{Interlayer mass}}{\text{Electrode mass without aluminum foil}} \times 100$$

However, it should be noted that most of the works utilizing interlayer in the above comparison table represents the sulfur content excluding the interlayer mass.

‘\*\*’ C-rate = mA g<sup>-1</sup>

‘\*\*\*’ Mass loading is in mg

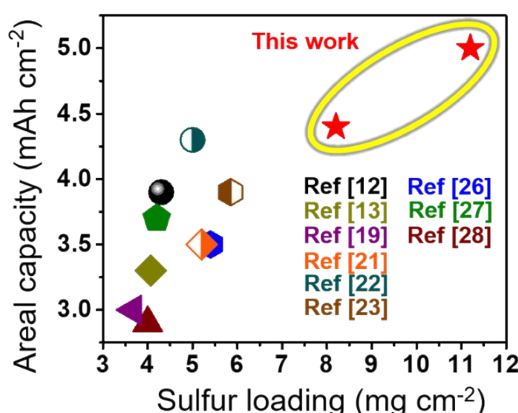


**Fig. S13.** Comparison of areal capacity versus sulphur loading values for N-CNF@VN/HNC interlayer obtained in the present work with previously reported results.

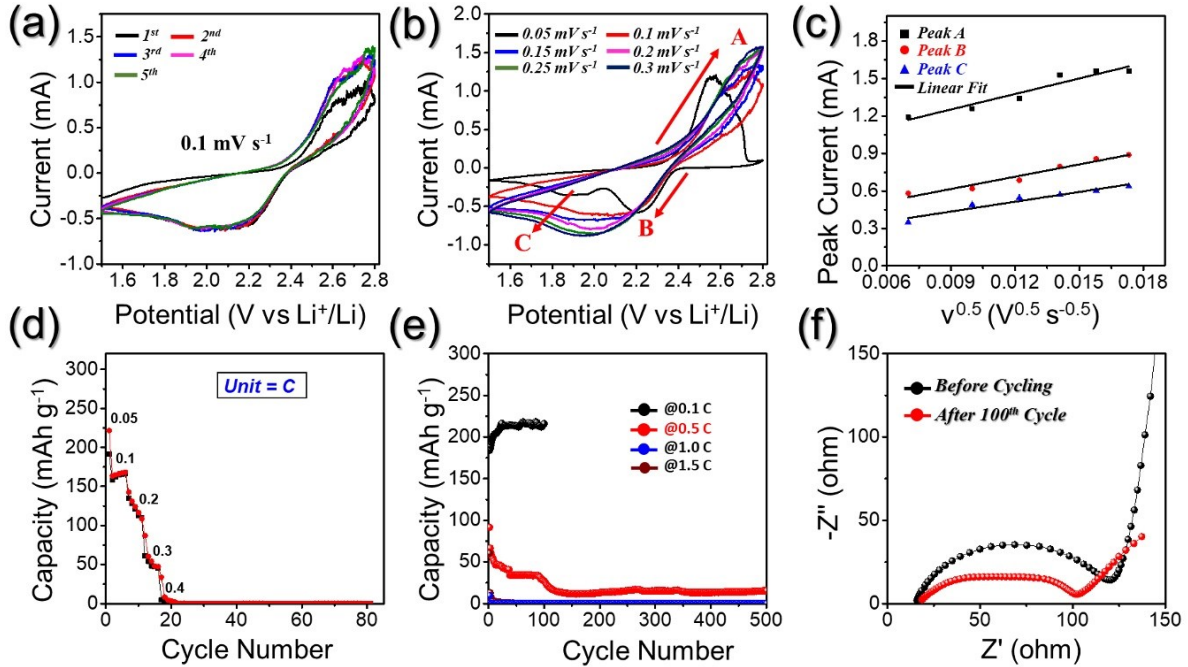


**Fig. S14.** Electrochemical performance of Li-S cells without interlayer: (a) initial five CV curves at  $0.1 \text{ mV s}^{-1}$ , (b,c) CV curves at different scan rates and their corresponding linear fits to the peak current values, (d) rate performance, (e) cycling performance at various C-rates, and (f) Nyquist impedance plots before and after cycling at 0.5 C-rate.

The electrochemical performance of Li-S cells assembled without interlayer is shown in Fig. S14. The CV curves obtained at a scan rate of  $0.1 \text{ mV s}^{-1}$  (Fig. S14a) shows broad cathodic peak at approximately 2.1 V and no obvious anodic peak, suggesting poor redox kinetics inside the cell. Besides, the low current values even at high scan rates (Fig. S14b) also indicates sluggish electrochemical processes. These results are well supported by the low value of lithium-ion diffusion coefficient (average  $D_{\text{Li}^+} = 9.7 \times 10^{-10} \text{ cm}^2 \text{ s}^{-1}$ ) calculated from the slope of peak current versus square root of scan rate curve (Fig. S14c). The poor rate capability (almost zero capacity after 0.4 C-rate) and substandard cycling performance shown in Fig. S14d and e, respectively, further validate the above results. Besides, a high charge transfer resistance ( $R_{\text{ct}}$ ) value of approximately  $100 \Omega$  and  $85 \Omega$  before and after cycling (Fig. S14f), respectively, implies poor charge transfer processes inside the cell. Overall, Li-S cell without interlayer display inferior electrochemical performance owing to inadequate immobilization of the lithium polysulfides.

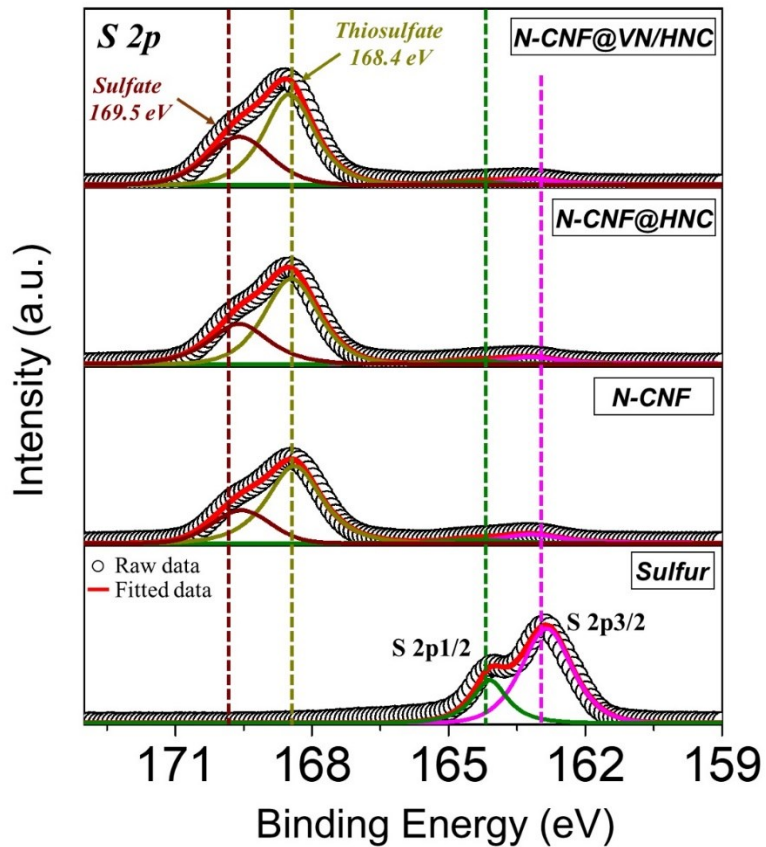


**Fig. S15.** S 2p XPS signal comparison for lithium polysulfide treated composite nanofibers along with the commercial sulfur.

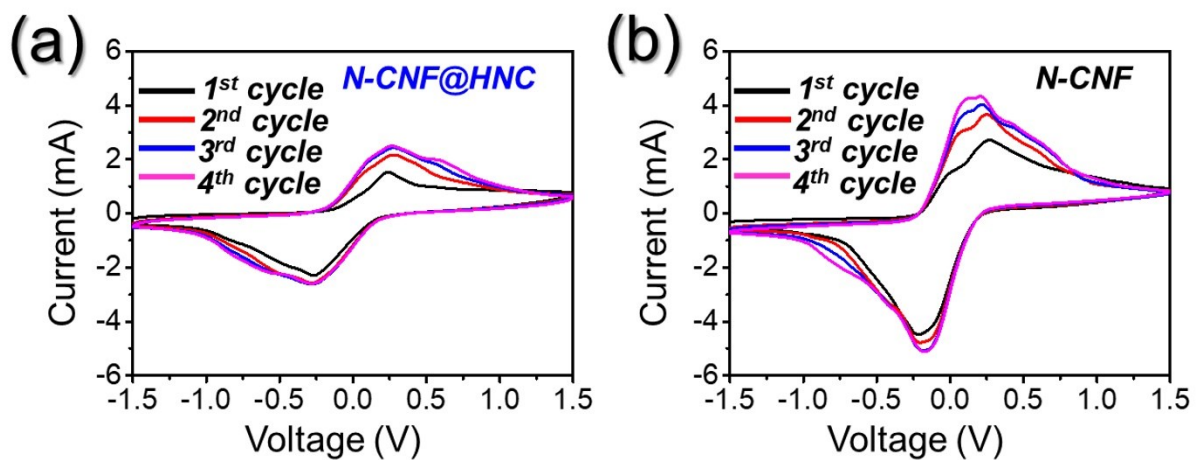


**Fig. S16.** First four CV cycles for (a) N-CNF@HNC and (b) N-CNF symmetric cells at 3 mV s<sup>-1</sup> from -1.5 to 1.5 V.

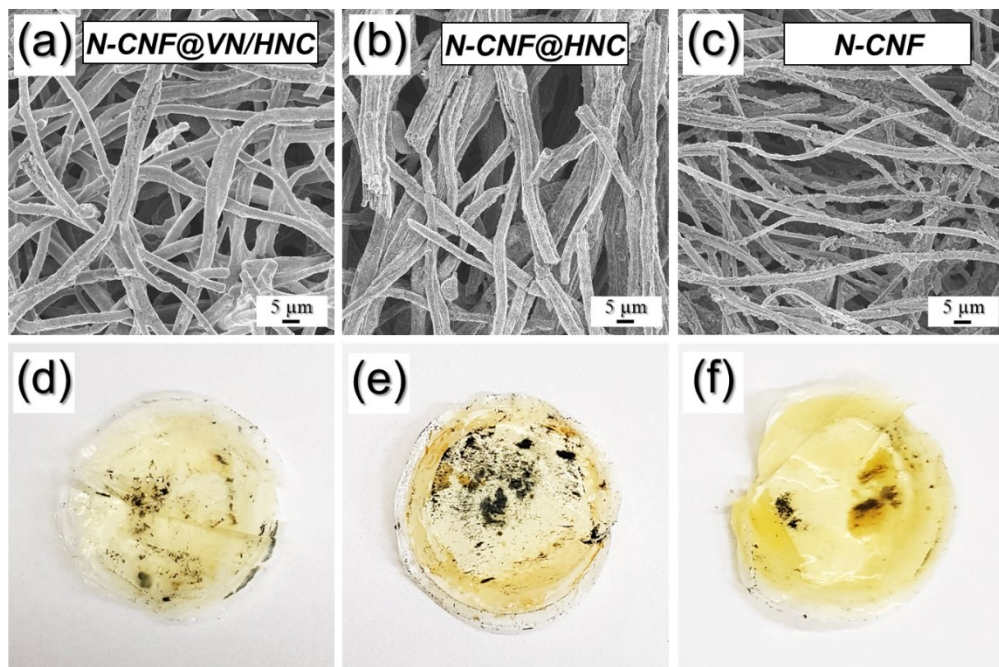


**Fig. S17.** The sulfur cathode facing-side FE-SEM images of the various freestanding interlayers along with the digital photographs of the Celgard separator after cycling at 1.0 C-rate. (a,d) N-CNF@VN/HNC interlayer, (b,e) N-CNF@HNC interlayer, and (c,f) N-CNF interlayer.

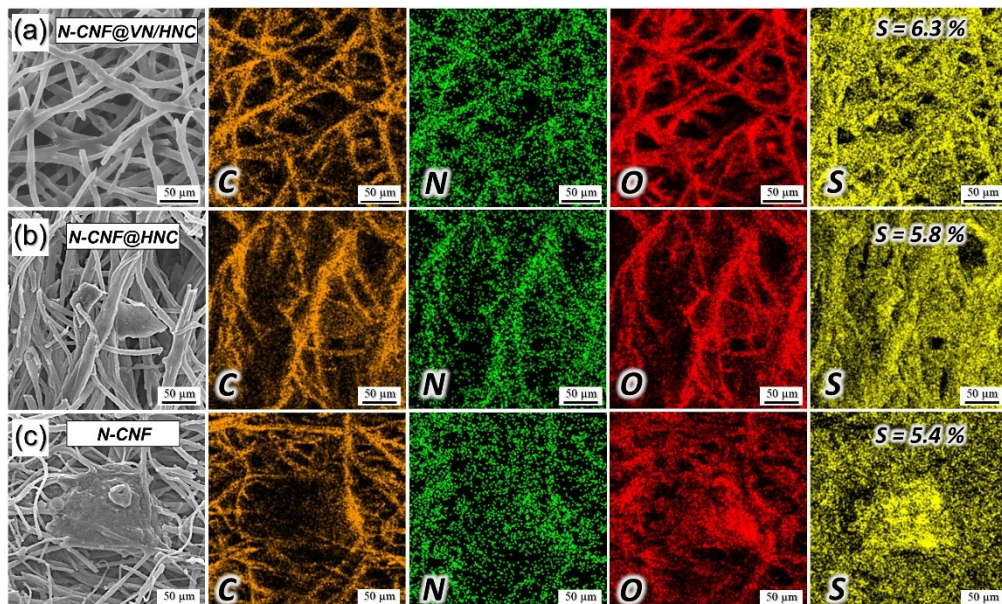


**Fig. S18.** Elemental mapping images of different freestanding interlayers after cycling at 1.0 C-rate. (a) N-CNF@VN/HNC interlayer, (b) N-CNF@HNC interlayer, and (c) N-CNF interlayer.

**Table S3.** Lithium-ion diffusion coefficient ( $D_{Li^+}$ ) calculated using Randles-Sevcik equation for cells with different interlayer arrangement.

Interlayer	$D_{Li^+} (\text{cm}^2 \text{s}^{-1}) \times 10^{-7}$			Avg. $D_{Li^+} (\text{cm}^2 \text{s}^{-1}) \times 10^{-7}$
	Peak A	Peak B	Peak C	
<b>N-CNF@VN/HNC</b>	2.76	0.56	1.49	1.60
<b>N-CNF@HNC</b>	3.07	0.47	0.87	1.47
<b>N-CNF</b>	1.67	0.52	0.85	1.01

## References

- 1 Y. Song, S. Zhao, Y. Chen, J. Cai, J. Li, Q. Yang, J. Sun and Z. Liu, *ACS Appl. Mater. Interfaces*, 2019, **11**, 5687-5694.
- 2 M.S. Garapati and R. Sundara, *Electrochim. Acta*, 2020, **362**, 137035.
- 3 H. Ahn, Y. Kim, J. Bae, Y.K. Kim and W.B. Kim, *Chem. Eng. J.*, 2020, **401**, 126042.
- 4 K. Wu, Y. Hu, Z. Cheng, P. Pan, M. Zhang, L. Jiang, J. Mao, C. Ni, Y. Zhang, Z. Wang, X. Gu and X. Zhang, *J. Alloys Compd.*, 2020, **847**, 156443.
- 5 A. Belgibayeva and I. Taniguchi, *J. Power Sources*, 2021, **484**, 229308.
- 6 S-H Moon, M-C Kim, J-H Choi, Y-S Kim, H. Kim and K-W Park, *J. Alloys Compd.*, 2021, **857**, 158236.
- 7 P. Rani, K. S. Kumar, A. D. Pathak and C. S. Sharma, *Appl. Surf. Sci.*, 2020, **533**, 147483.
- 8 D. Park, S. Park and D-W Kim, *Chem. Eng. J.*, 2021, **405**, 126596.
- 9 B. Zheng, L. Yu, N. Li and J. Xi, *Electrochim. Acta*, 2020, **345**, 136186.
- 10 P. Wang, Z. Zhang, B. Hong, K. Zhang, J. Li and Y. Lai, *J. Electroanal. Chem.*, 2019, **832**, 475.

- 11 X. Yang, H. Zu, L. Luo, H. Zhang, J. Li, X. Yi, H. Liu, F. Wang and J. Song, *J. Alloys Compd.*, 2020, **833**, 154969.
- 12 Z. Sun, Y. Guo, B. Li, T. Tan and Y. Zhao, *Solid State Sci.*, 2019, **95**, 105924.
- 13 S. Jiang, M. Chen, X. Wang, Y. Zhang, C. Huang, Y. Zhang and Y. Wang, *Chem. Eng. J.*, 2019, **355**, 478-486.
- 14 X-Y Yue, X-L Li, J-K Meng, X-J Wu and Y-N Zhou, *J. Power Sources*, 2018, **397**, 150-156.
- 15 P. Guo, D. Liu, Z. Liu, X. Shang, Q. Liu and D. He, *Electrochim. Acta*, 2017, **256**, 28-36.
- 16 L-B Xing, K. Xi, Q. Li, Z. Su, C. Lai, X. Zhao and R. V. Kumar, *J. Power Sources*, 2016, **303**, 22-28.
- 17 J. Wang, Y. Yang and F. Kang, *Electrochim. Acta*, 2015, **168**, 271-276.
- 18 H. Tang, S. Yao, S. Xue, M. Liu, L. Chen, M. Jing, X. Shen, T. Li, K. Xiao and S. Qin, *Electrochim. Acta*, 2018, **263**, 158-167.
- 19 D. Wang, Q. Cao, B. Jing, X. Wang, T. Huang, P. Zeng, S. Jiang, Q. Zhang and J. Sun, *Chem. Eng. J.*, 2020, **399**, 125723.
- 20 J. Li, C. Jiao, J. Zhu, L. Zhong, T. Kang, S. Aslam, J. Wang, S. Zhao and Y. Qiu, *J. Energy Chem.*, 2020, **57**, 469-476.
- 21 J. Wang, T. Wu, S. Zhang, S. Gu, J. Jin and Z. Wen, *Chem. Eng. J.*, 2018, **334**, 2356-2362.
- 22 Q. Zhao, Q. Zhu, Y. An, R. Chen, N. Sun, F. Wu and B. Xu, *Appl. Surf. Sci.*, 2018, **440**, 770-777.
- 23 J. Han, Q. Fu, B. Xi, X. Ni, C. Yan, J. Feng and S. Xiong, *J. Energy Chem.*, 2021, **52**, 1-11.
- 24 W. Xu, X. Pan, X. Meng, Z. Zhang, H. Peng, J. Liu and G. Li, *Electrochim. Acta*, 2020, **331**, 135287.

- 25 X. Li, K. Ding, B. Gao, Q. Li, Y. Li, J. Fu, X. Zhang, P.K. Chu and K. Huo, *Nano Energy*, 2017, **40**, 655-662.
- 26 Y. Zhang, K. Li, H. Li, Y. Peng, Y. Wang, J. Wang and J. Zhao, *J. Mater. Chem. A*, 2017, **5**, 97-101.
- 27 L. Zhu, C. Li, W. Ren, M. Qin and L. Xu, *New J. Chem.*, 2018, **42**, 5109-5116.
- 28 W. Ren, L. Xu, L. Zhu, X. Wang, X. Ma and D. Wang, *ACS Appl. Mater. Interfaces*, 2018, **10**, 11642.